Investigation on the removal characteristics of single-point cutting high-volume fraction SiCp/Al composites

Yongjie Bao
Dalian Maritime University
Xu Zhang
Dalian University of Technology
Shouxiang Lu
Southern University of Science and Technology
Hongzhe Zhang (zhanghongzhe@dlut.edu.cn)
Dalian University of Technology

Research Article

Keywords: SiCp/Al composites, SiC particles, removal characteristics, finite element model, single grit cutting, Cutting mechanism, Metal matrix composite, Surface quality

Posted Date: April 1st, 2021

DOI: https://doi.org/10.21203/rs.3.rs-159623/v1

Version of Record: A version of this preprint was published at The International Journal of Advanced Manufacturing Technology on September 9th, 2021. See the published version at https://doi.org/10.1007/s00170-021-07977-5.

Investigation on the removal characteristics of single-point cutting high-volume fraction SiCp/Al composites

Yongjie Bao[1], Xu Zhang[2], Shouxiang Lu[3], Hongzhe Zhang[2*]

1. Marine Engineering College, Dalian Maritime University, Dalian 116026, China

2. Engineering Training Center, Dalian University of Technology, Dalian 116024, China

3. Department of Mechanical and Energy Engineering, Southern University of Science and Technology, Shenzhen 518055, China

*Corresponding author. E-mail address:zhanghongzhe@dlut.edu.cn (Hongzhe Zhang)

Abstract: SiC reinforced aluminum matrix composites (SiCp/Al composites) are typical difficult-to-machine material, and the irregular SiC particles diffused in SiCp/Al composites make the surface quality worse. In this paper, a single-point cutting investigations with finite element simulation were conducted for 65% SiCp/Al composites and aluminum alloy. The surface morphology characteristics of SiCp/Al composites, which mainly include breaking, part breaking, pulling out, protruding, al tearing, and interface debonding, are different from those of aluminum alloy materials. The high-volume SiC particles lower the surface quality and profile dimensional accuracy of SiCp/Al composites. There are thin and discrete layers covered on the machined surface.

Keywords:

SiCp/Al composites, SiC particles, removal characteristics, finite element model, single grit cutting, Cutting mechanism, Metal matrix composite, Surface quality

1 Introduction

SiCp/Al composites with high SiC particles volume fraction have excellent physical and mechanical properties, including high specific strength, high specific modulus, good wear resistance, high temperature resistance, low thermal expansion coefficient and good dimensional stability [1-3]. SiCp/Al composites are widely used in aerospace industry, automotive industry, electronics industry and other fields [4-6]. However, due to clustering and non-homogeneous distribution of hard SiC particles in the ductile aluminum alloy matrix, SiCp/Al composites have poor machinability. Both failure criteria and mechanical behaviors are different from homogeneous materials during the machining process. The material is a kind of typical difficult-to-machine material, which is easy to cause numerous surface defects and rapid tool wear rate in cutting process [7-11]. All of these make the machining of SiCp/Al composites challenging. Therefore, the study on cutting characters of SiCp/Al composites has become a hotspot.

At present, numerical modeling has been used by many researchers as a tool to understand the SiCp/Al composites removal mechanisms associated with machining processes. Wang et al. [12] studied the influences of fracture and removal mechanism of SiC particles on surface generation using a three-dimensional (3D) finite element model of turning. It was found that the manners of SiC particulates removal have an important influence on surface generation. Liu et al. [13] and Wu et al. [14] using the finite element models studied the material removal mechanism and defect formation mechanism

of SiCp/Al composites considering tool and SiC particles interaction in different positions. The results showed that the major material removal form of SiC particles is brittle fracture and pulling out base on the different area of SiC particles in contacting with the tool. Xiang et al. [15] combined turning finite element analysis with ultrasonic assisted milling experiment and found that the application of ultrasound improved the particle rupture effect. An appropriate ultrasonic amplitude inhibited the particle breakage and slowed down the crack growth. A smoother particle breaking phenomenon was observed with the application of a higher frequency. Wang et al. [16] investigates the underlying cutting mechanism of SiC particle-reinforced aluminum matrix composites (MMCs) using finite element (FE) simulations and precision turning experiments. The results indicated that the particle size has significant influence on the surface quality of the machine surface of SiCp/Al MMCs and the fracture and removal of particle shows significant effect on the surface generation.

The single-point cutting test is an effective method to study the removal characteristics of particles reinforced metal matrix composites. Yan et al. [17] studied the cutting mechanisms and the relationship between specific energy of scratching and depth of cut (size effect) on low volume fraction (10%-20%) composites reinforced by $A1_20_3$ and SiC ceramic particles by single point cutting test. The results indicated that the scratch process was composed of rubbing, ploughing, plastic and for machining MMCs, a larger depth of cut should be used to maintain a lower machining energy, especially for those with a larger ratio of volume fraction to particle radius. Feng et al. [18] and Zha et al. [19] studied the scratch load, coefficient of friction (COF) and scratch morphology on 55% SiCp/Al composites by comparing the ultrasonic vibration-assisted scratch (UVAS) and traditional scratch tests. The results indicated that the ultrasonic vibration played an important role in reducing the grinding force and COF, as well as improving the morphology of the machined surfaces.

There is very little literature regarding the single-point cutting of higher volume fraction (greater than 55%) SiCp/Al composites. The volume fraction increasing makes the cutting process more complicated. The material removal mechanism of high volume fraction SiCp/Al composites still need further study. The material removal process is difficult to be directly observed due to the random distribution of different sized abrasive particles. Therefore, the single-point cutting test can be used to simplify the cutting process so that the material removal mechanism can be better revealed. And the finite element simulation can be used to reveal the material removal process in microscopic view and the elastic, plastic deformation and fracture process of SiCp/Al composites can be revealed.

In this paper, the surface formation process of 65% SiCp/Al composites was studied. A single-point cutting investigations with finite element simulation were conducted. Compared with aluminum alloy, the cutting property and surface generation characteristics of 65% SiCp/Al composites were revealed.

Nomenclature

		ε_f	fracture strain
		η	stress triaxiality
σ	flow stress (Mpa)	p	pressure stress(Mpa)
A	yield stress at reference	q	von Mises equivalent stress (MPa)

	temperature and strain rate (Mpa)		
B	strain hardening coefficient (Mpa)	ε_p	plastic strain rate
ε	plastic strain	ε_0	reference strain rate
n	the strain hardening exponent	T_r	transition temperature defined as the one at or below which there is no temperature dependence on the expression of the fracture strain (K)
m	thermal softening exponent	σ_1, σ_2, σ_3	principal stresses in three directions respectively(Mpa)
$\overline{\varepsilon}$	strain rate	σ_p	tensile strength of material(Mpa)
ε_0	reference plastic strain rate	τ	friction force(N)
T	workpiece temperature(K)	P	positive pressure(Mpa)
T_m	material melting temperature(K)	σ_b	tensile strength of material
T_{room}	room temperature(K)	μ_{n0}	normal displacement at failure
d_1-d_5	Failure parameters of matrix materials	G_f^I	mode I fracture energy
w_D	scalar of failure state	σ_{tu}^I	failure stress
$\Delta\varepsilon_p$	equivalent plastic strain during each integration cycle	G_s	shear modulus after the crack opening
μ	coefficient of sliding friction	G	shear modulus of the undamaged material
$\rho(e_{nn}^{ck})$	shear retention factor of material	e_{nn}^{ck}	cracking opening strain
p	material parameters	e_{max}^{ck}	material parameters

2 SiCp/Al composites removal model

2.1 Finite element model

A microstructure-based two-dimensional plane strain and random particle single point cutting model was built with Abaqus/Explicit by imitating the real particle morphology from typical micrographs of 65%SiCp/Al composites, as shown in the upper half of **Fig. 1**. In this model, the volume fraction of SiC particle in SiCp/Al composites is 65% and the SiC particles exhibited an average size of about 40 μm. The workpiece length and height are 1.6 mm and 0.4 mm. The cone vertex angle and radius of the single diamond grit is 120◦ and 0.2 mm respectively. The cutting speed is 5.26m/s, and the cutting path is circular arc. The maximum cutting depth 20 μm is available in the bottom of the circular arc. It can also be seen that the morphology of the SiC particles, which agrees with typical micrographs of 65%SiCp/Al composites, is polygonal, including quadrilateral, pentagon and hexagon. In order to simplify the algorithm, the volume fraction is defined as the ratio of sum of polygon areas and workpiece area. The model of the workpiece is generated by a custom subroutine which can automatically build model of workpiece by setting some model parameters, such as sic particles shape, diameter and volume fraction. The custom subroutine also enables random distribution of particles in the matrix. In the simulation, the random distribution of particles can truly reproduce the microstructure of the composite; the interaction between particles can also be fully considered [20]. In this model, the matrix and the particles were modeled separately and the 4-node plane strain bilinear quadrilateral elements (CPE4RT) in ABAQUS were

adopted to mesh both the matrix and SiC particles. The global element size of 0.0055 mm was selected. Since the interface is very hard and brittle and hence similar to the particles [21], the interface was considered as an extension of the particle. The particle and the matrix are tied together so that their initial displacements at the interface are equal. The interfacial debonding is achieved through the failure of the matrix material which is also used by other researchers [22-25].

The tool used in this experiment is a standard diamond indenter, and it is simplified in the simulation. Because the tool has the characteristics of high hardness, strength, wear resistance, and high temperature resistance, less deformation occurred during machining process. It is established to the rigid body, to improve the calculation efficiency. And the reference point is set on the tool to control the tool cutting path and output the cutting force and other parameters.

Penalty contact between the cutting tool with matrix and particles is defined with the aim of enabling the tool-particle interaction. The workpiece is constrained at bottom and sides surface. Furthermore, a two-dimensional plane strain model of aluminum alloy (0 vol %) was also built to compare with the SiCp/Al composites (65 vol %), as shown in the bottom half of **Fig. 1**. The main difference between the model of 2a12 aluminum alloy and SiCp/Al composites is whether the workpiece contains sic particles or not. Through comparative analyses of material removal processes, the influence of SiC particles on surface generation of SiCp/Al composites can be revealed.

In this work, the single point geometric parameters, cutting path, maximum cutting depth, cutting speed, average particle size, volume fraction and so on are all comparable to the experimental data.

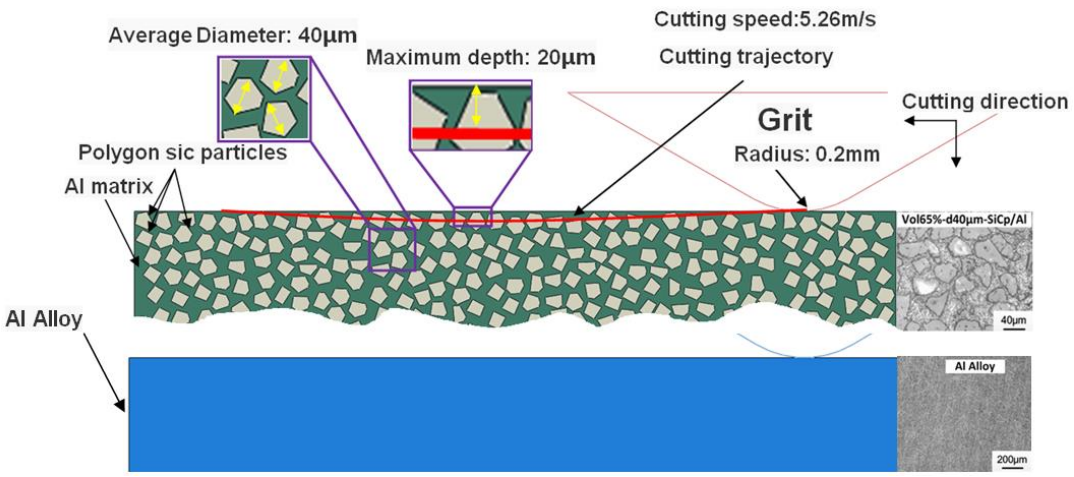

Fig. 1 Finite element model of single point cutting of 65% SiCp/Al composites and 2A12 aluminum alloy

2.2 Material constitutive equation

Aluminum alloy has flow characteristics and is greatly influenced by strain, strain rate and high temperature. Johnson–Cook constitutive equation includes those influence factors. Thus, it can well simulate the cutting process of matrix materials in practice. In this work, the Johnson–Cook constitutive equation was implemented to model the flow behavior of Al alloy. Here, the Johnson–Cook model can be expressed as:

$$\sigma=\left[A+B\varepsilon^{n}\right]\left[1+C\ln\left(\frac{\bar{\varepsilon}}{\varepsilon_0}\right)\right]\left[1-\left(\frac{T-T_r}{T_m-T_r}\right)^{m}\right]$$

(1)

Where σ is the flow stress, A is the yield stress at reference temperature and strain rate, B is the strain hardening coefficient, ε is the plastic strain, n is the strain hardening exponent, C is the strain rate sensitivity coefficient, and m is the thermal softening exponent, $\dot{\bar{\varepsilon}}$ is the strain rate, ε_0 is the reference plastic strain rate. T is the workpiece temperature, and T_m and T_r are the material melting and room temperature, respectively.

The material constants of 2A12 Al alloy matrix are obtained from the split Hopkinson pressure bar (SHPB) test over wide temperatures and strain rates by Li [26] and listed in **Table 1**. The material parameters of Al alloy matrix and silicon carbide applied in the finite element computational analysis are listed in **Table 2** [26-28].

Table 1 Material constants for Johnson–Cook constitutive model of 2A12 Al alloy

A/MPa	B/MPa	n	C	m	T_{melt}/K
370.4	1798.7	0.73315	0.0128	1.5282	863

Table 2 Material parameters of 2A12 Al alloy and SiC

Material parameters	2A12	SiC
E, Young's modulus (GPa)	71.7	420
μ, Poisson's ratio μ	0.33	0.14
Coefficient of thermal expansion (K^{-1})	26.6×10^{-6}	4.9×10^{-6}
ρ, Density($kg\cdot m^{-1}$)	2.77×10^{3}	3.13×10^{3}
k, Thermal conductivity/($W\cdot m^{-1}\cdot K^{-1}$)	175	81
C,specific heatC/($J\cdot kg^{-1}\cdot K^{-1}$)	921	427

2.3 Fracture criterion of matrix material

Liu.et all [29] found that the simulation results agreed well to the experiment results of metal cutting process when using the Johnson–Cook damage criterion including failure evolution model. Thus, in this work, Johnson–Cook damage criterion was utilized to describe the chip separation behavior for all the Al alloy matrix elements. Johnson–Cook criterion for damage initiation is met when the following condition is satisfied [30]:

$$w_D = \sum \frac{\Delta\varepsilon^p}{\varepsilon_f} = 1 \tag{2}$$

$$\varepsilon_f = \left[d_1 + d_2 \exp\left(-d_3\eta\right)\right]\left[1 + \ln\left(\frac{\varepsilon^p}{\varepsilon_0}\right)\right]\left[1 + d_5\left(\frac{T - T_r}{T_m - T_r}\right)\right] \tag{3}$$

Here, w_D is scalar of failure state, $\Delta\varepsilon^p$ is the change in the equivalent plastic strain during each integration cycle, ε_f is the fracture strain, d_1-d_5 are the failure parameters of matrix materials, $\eta=p/q$ is the stress triaxiality, p is the pressure stress, q is the von Mises equivalent stress, ε^p and ε_0 are the plastic strain rate and reference strain rate respectively. T and T_m are the workpiece temperature and melting temperature, and T_r is the transition temperature defined as the one at or below which there is no temperature dependence on the expression of the fracture strain ε_f [30]. In addition, the SiC particles are modeled as an isotropic and perfectly elastic material following the generalized Hook's Law, and brittle cracking model was used. The failure parameters d1−d5 applied in the Abaqus/Explicit are listed in **Table 3** [28].

Table 3 Johnson–Cook damage parameters of 2A12 Al alloy matrix

d1	d2	d3	d4	d5
0.116	0.211	-2.172	0.012	-0.01256

2.4 Fracture criterion of SiC material

In this paper, the brittle fracture criterion was added into the material property of SiC to simulate the cracking of SiC particles in cutting process. SiC particles are hard and in elastic state before fracture, and he relationship of stress and strain obeys the generalized Hook's law. The judgement of fracture initiation is maximum normal stress criterion [31]. The formula can be expressed as:

$$\max\left(\sigma_1,\sigma_2,\sigma_3\right)=\sigma_b \tag{4}$$

Here, σ_1, σ_2 and σ_3 are principal stresses in three directions respectively. σ_b is tensile strength of material. The crack is assumed to initiate if the max (σ_1, σ_2, σ_3) is greater than or equal to σ_b.

After the initiation of crack, fracture energy criterion is used to control the degradation of tension stiffening, and the crack normal displacement at failure is defined as [31]:

$$\mu_{n0}=2G_f^{I}/\sigma_{tu}^{I} \tag{5}$$

Here, μ_{n0} is the normal displacement at failure, G_f^{I} is the mode I fracture energy, and σ_{tu}^{I} is the failure stress.

A function of the crack opening strain about the shear retention model is defined to describe the damage development of sic particle caused by shear stress. The shear modulus after the crack opening is G_s and it can be calculated by the following formula [31]:

$$G_s=\rho(e_{nn}^{ck})G \tag{6}$$

Here, G is the shear modulus of the undamaged material, and ρ (e_{nn}^{ck}) is the shear retention factor of material, which can be calculated by the following formula [31]:

$$\rho(e_{nn}^{ck})=(1-\frac{e_{nn}^{ck}}{e_{\max}^{ck}})^{p} \tag{7}$$

Here, e_{nn}^{ck} is the cracking opening strain; p and e_{max}^{ck} are material parameters [32]. The parameters about the material fracture model are listed in **Table 4** [33].

Table 4 Parameters of the material fracture model

σ_b (Mpa)	G_f^{I} (J/m^2)	p	e_{max}^{ck}
1500	30	1	0.001

2.5 Friction model

The friction between the tool and the workpiece has great effect on cutting force and cutting temperature, thus affecting the surface integrity. Therefore, the selection of friction model is very important for guaranteeing a high-quality calculation. The chip of high-volume fraction SiCp/Al composites has high brittleness, and the tool-chip relative sliding is more remarkable than tool-chip coalescence. Therefore, coulomb friction model is applied into the interaction between the tool and the matrix material as well as the tool and SiC particles. The formula can be expressed as:

$$\tau=\mu P \tag{8}$$

Here, τ is friction force, μ is coefficient of sliding friction and P is positive pressure. A constant Coulomb friction coefficient of

μ=0.5 is used in all simulations since it represents sliding contact condition between the tool and the workpiece [34].

2.6 Simulation results of single point cutting

Aluminum alloy has good plasticity and low hardness while SiC is hard and brittle. SiCp/Al composites contain both aluminum alloy and SiC particles, which makes the cutting process complex. Especially for high-volume fraction SiCp/Al composites, the cutting characteristics needs to be further revealed. Thus, single point cutting simulation was carried out on the three materials for revealing the influence of volume fraction on cutting quality through comparative analyses.

Fig. 2 shows the surface topography of aluminum alloy after single point cutting simulation. It can be seen that aluminum alloy has good surface integrity and no defects like pits or cracks after cutting. Furthermore, there is only plastic deformation and few scales, and the fluctuation of the contour is small.

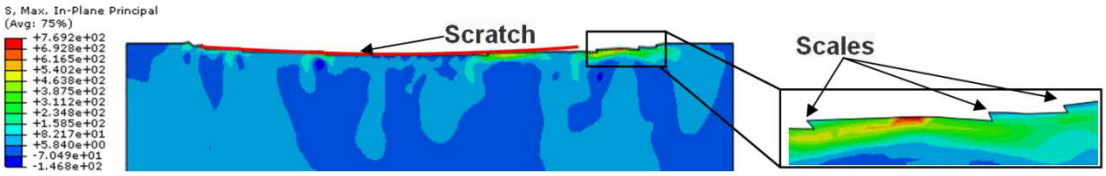

Fig. 2 Removal models of 2A12 aluminum alloy materials

Fig. 3 shows the surface topography of 65% SiCp/Al composites. It can be found that the high-volume fraction of SiC particles increase the brittleness of material and the material surface has defects like interfacial debonding (**Fig. 3a**), protruding(**Fig. 3b**), pulling out(**Fig. 3c**), crushing(**Fig. 3d**), part crushing(**Fig. 3f**), al tearing(**Fig. 3e**) and so on. As a whole, the cutting surface presents an uneven surface topography including pits, protruding and plastic deformation, severely affecting the surface quality. The cutting surface of SiCp/Al composites is very different from aluminum alloy. The addition of SiC particles changes the materials removal mechanism. There are both plastic failure of aluminum matrix and brittle failure of SiC particles in the failure procedures of SiCp/Al composites. Furthermore, because of the high hardness of SiC particles, it generates pushing effect on aluminum alloy, causing the appearance of micro-cracks and deformation on the surface topography.

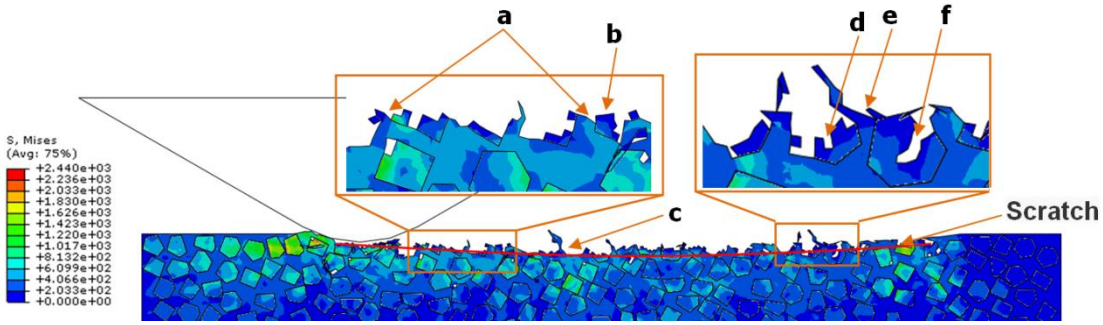

Fig. 3 Removal models of 65% SiCp/Al composites

3 Single point cutting experiment

In order to reveal the material removal characteristics, single point cutting experiments were carried out on aluminum

alloy and 65% SiCp/Al composites. The scratch appearance and micro morphology were observed, and the characteristics of material failure were analyzed.

3.1 Pretreatment of materials

The materials used in the experiments were 2A12 aluminum alloy and 65% SiCp/Al composites. The mean diameter of the SiC particles is 40 um. In order to reduce the effects of surface roughness and residual stress on experimental results, rotation and gravity type of grinding-and-polishing machine was utilized to grind and polish the materials. The average roughness of all test workpieces is less than 0.05 μm after the pretreatment and the surface topography pictures were shown in **Fig. 4**.

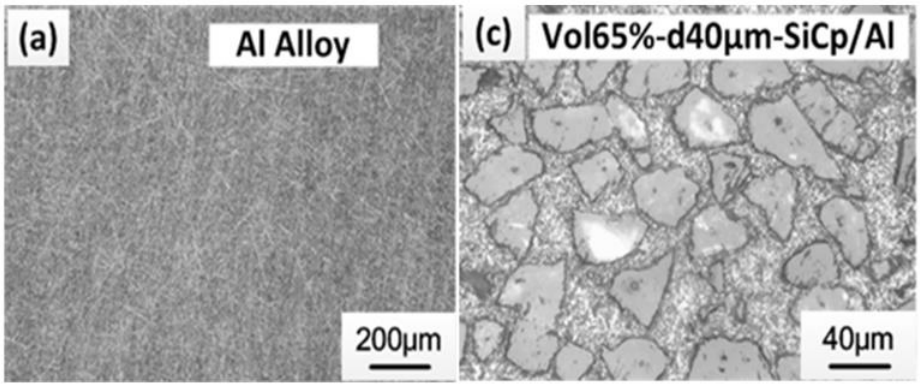

Fig. 4 Surface topography of test pieces after pretreatment

3.2 Experimental details

The experiments were carried out on CNC drilling and milling test bench, and the testing apparatus is shown in **Fig. 5**.

It can be seen that the disc-like aluminum alloy cutterhead is clamped in the end of motorized spindle. The rockwell hardness indenter is fixed on the columned clamp holder and is connected with aluminum alloy cutterhead through screw threads. In the experimental speed range, in order to make the tool and the fixture in a dynamic balancing state, a clump weight is installed on the columned clamp holder symmetrically to the aluminum alloy cutterhead. Workholder is fixed on the Kistler 9257b three-component dynamometer and the latter is fixed on the machine table, linking with computer through charge amplifier and data acquisition card.

During experiments, the machine spindle rotates and the rotating speed is n. In order to ensure that the scratch on the test specimen is only through one cutting, the relative motion between the test specimen and the tool should be reasonably controlled. The machine tool feed movement process undergoes acceleration and uniform motion stage successively. The acceleration time or deceleration time of the feed movement of the tool is 0.1 s, and the acceleration distance or deceleration distance is 5 mm. Thus, the distance between the diamond grit tip of rockwell hardness indenter and test specimen is 5 mm after tool setting, as shown in **Fig. 6**. The cutting depth is set as h. The machine spindle moves to a specified position at a speed of v_f and stops for holding Δt seconds, and then moves back to the initial point at a speed of - v_f. In addition, the holding time is crucial, because if the Δt is too large, the frequency of exposure between the tool and the test specimen will be more than once. While, if the Δt is too small, the tool will not be in contact with the test specimen. Thus, Δt

should be determined appropriately under the corresponding spindle speed, ensuring the frequency of exposure between tool and test specimen to be only once. In order to investigate the detailed interface profile and surface morphology, KEYENCE VK-X250 laser scanning confocal microscope (LSCM) and FEIQ45 scanning electron microscope (SEM) were used to examine the surface of the samples. The parameters of single point dicing are shown in **Table 5**.

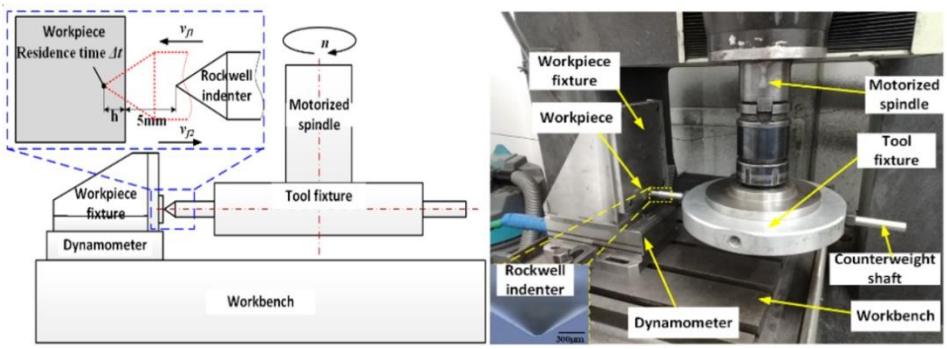

Fig. 5 The method of dicing test and testing apparatus

Table 5 The parameters of single point dicing

Cutting depth h/μm	Cutting radius r/mm	Cutting speed /(m·s^{-1})	V_s	Holding time Δt/s	Feed speed V_f/(mm·min^{-1})
20	162	5.26		0.1~0.15	100

4 Experimental results and discussions

4.1 Cutting force

In order to validate this model, a comparison was made between the simulated and experimental measurements of the cutting force. The maximum, minimum and average values of cutting force were calculated from the data based on the simulation and experiment, as shown in **Table 6**. The average cutting force error of Al alloy and SiCp/Al is 8.67% and 8.06% respectively. By calculating the average cutting force error of simulation and experiment, which is also used by Zhou et al. [34], can prove that simulation model is reasonable.

Table 6 Material parameters of 2A12 Al alloy and SiC

Cutting force	Maximum(N)	Minimum(N)	Average(N)	Average error(%)
Al alloy(simulation)	20.6244	2.3504	12.2999	8.67
Al alloy(experiment)	18.7298	0.5215	11.3194	
SiCp/Al(simulation)	32.1861	1.18098	15.1241	8.06
SiCp/Al(experiment)	23.9737	0.2536	13.9960	

4.1 Overall surface topography

The overall surface topography of the three materials is shown in **Fig. 6**. It can be seen that the scratch appearance of aluminum alloy is clear. Material accumulation appeared on both sides of scratch centerline showing plastic flow features. In the case of 65% SiCp/Al composites, material accumulation also occurs on both sides of scratch centerline. However, the centerline is poor than

aluminum alloy, and the accumulation of materials is discontinuous, having low surface flatness. The overall surface topography of the two materials matches the simulation well. Aluminum alloy has good plastic-flow features, and there are common phenomena in metal cutting process, such as scraping, ploughing and cutting. In the case of 65% SiCp/Al composites, although the aluminum matrix still has plasticity features, the addition of SiC particles increases the brittleness of SiCp/Al composites and causes the low surface flatness. It can be seen that the increase of volume fraction of SiC particles will decrease the surface quality of cutting.

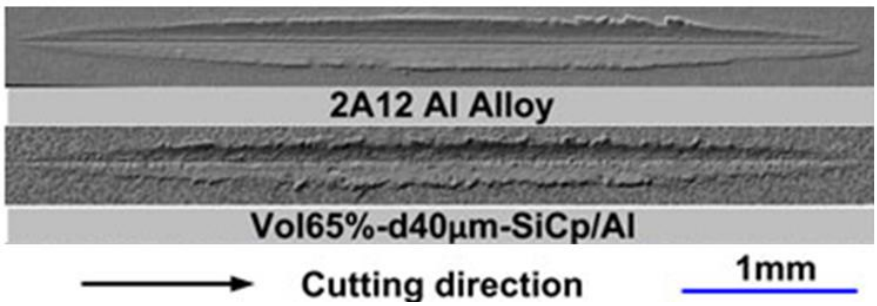

Fig. 6 The overall appearance of three materials after dicing

4.2 Morphology of longitudinal cross-section

The scratch profile curves of the two materials were measured by confocal laser scanning microscope. The profile variation is shown in **Fig. 7a**. Part 'b', 'c' and 'd' marked in **Fig. 7a**, correspond to the cut-in parts (**Fig. 7b**), maximum cutting depth parts (**Fig. 7c**) and cut-out parts (**Fig. 7d**). **Fig. 7b, c** and **d** are partially enlarged part of the **Fig. 7a**. It can be seen that the scratch profile curve of aluminum alloy is most similar to the nominal profile curve among the two materials. The profile integrity is good and the profile fluctuation is small. However, the scratch profile curve of 65% SiCp/Al composites obviously deviates from the nominal profile curve and the range of profile variation is obviously wider than aluminum alloy. It shows that the addition of SiC particles increases the brittleness of SiCp/Al composites and the brittle fracture causes the remarkable profile fluctuation. Thus, the profile integrity of 65% SiCp/Al composites is worse than aluminum alloy as well.

From further analyses of cut-in parts (**Fig. 7b**), maximum cutting depth parts (**Fig. 7c**) and cut-out parts (**Fig. 7d**), it can be seen that, in the initial cut-in stages, the plastic deformation of aluminum alloy occurred under the action of tool, and the profile dimension is similar to nominal profile dimension. Since the SiC particles increase the hardness of SiCp/Al composites, the amount of deformation in the initial stage is small and the fluctuation of deformation increases with the deepening of the tool. It can be seen that From the **Fig. 7,** the profile fluctuation range of aluminum alloy is about 3 μm, but the profile fluctuation range of SiCp/Al composites, which is almost 3 times of the aluminum alloy, is about 8 μm. In maximum cutting depth parts (**Fig. 7c**), the profile curve of aluminum alloy is almost as same as the nominal profile curve and the profile fluctuation is very small, the profile fluctuation range reaching its minimum. However, the profile fluctuation of SiCp/Al composites is big and the profile fluctuation range reaches its maximum. The reason for the phenomenon is that, at maximum cutting

depth part, in the process of cutting, plastic deformation was mainly undergone in aluminum alloy, but brittle fractures was mainly undergone in SiCp/Al composites.

From the longitudinal section morphology of the scratch, it can be seen that the fluctuation of profile curve of the SiCp/Al composites increases with the addition of SiC particles. The cutting quality of SiCp/Al composites is obviously lower than aluminum alloy, indicating that the simulated analysis matches the test well.

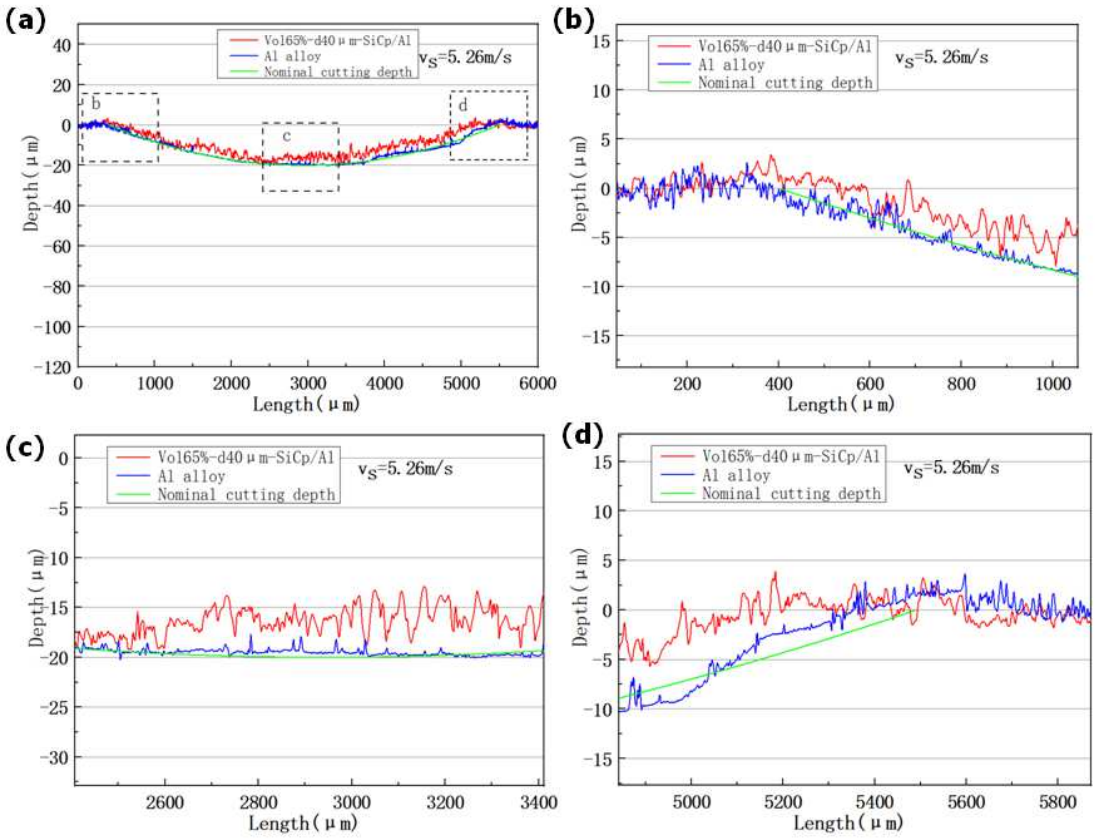

Fig. 7 The scratch profile dimensions of three materials after dicing

4.3 Scratch morphology

The surface topography of the three kinds of cut specimens was examined to reveal the removal characteristics of SiCp/Al composites by comparative analyses.

The results of cutting simulations are compared to single point cutting experimental results, as shown in **Fig. 8a** and **b**. It can be seen that except for plastic deformation, some scales were found on the surface of 2A12 Al. The reason for the generation of scales is considered that the tension stress in the cutting process may induce crack growth and so scales damage appear on the surface of workpiece, as shown in the **Fig. 8c** and **d**. Furthermore, in cutting process of SiCp/Al composites, the scale phenomenon will induce defects like Al tearing and interface debonding.

The simulation and experimental results of SiCp/Al composites are shown in **Fig. 8e-n**. The phenomena of interfacial debonding and SiC particles cleavage can be seen from **Fig. 8e** and **f**. It is because that there can be randomly scattered original micro-cracks on the surface of SiC particles, being very easy to cause cracks growth under the squeezing action of tool. This can cause cleavage

phenomenon on the surface of SiC particles and make the aluminum alloy matrix squeezed, causing plastic deformation in the direction of weak restrictions and concentrates stress between the interface of aluminum alloy matrix and SiC particles. Furthermore, when the stress exceeds the interfacial limit strength, there can be the phenomena of interfacial debonding. Furthermore, the large tensile stress will also lead to interfacial debonding, as same as the mechanism of scale phenomenon in 2A12 Al.

The phenomena of microcracks, SiC particle breakage and Al-matrix tearing can be seen from **Fig. 8g** and **h**. With the interaction between abrasive particle and material, the large tensile stress behind the abrasive particle will lead to micro-crack initiation and Al-matrix tearing. According to indentation fracture mechanics, if the normal stress in contact-position of SiC particles exceeds the fracture strength, it will cause median and lateral cracks. With the movement of abrasive particle, the horizontal crack extends to the surface and causes the breakage of Sic particles.

The phenomena of SiC particles protruding and pulling out can be seen from the **Fig. 8i** and **j**. With the movement of abrasive particle, if the interfacial strength of upper half of the SiC particles much larger than the bottom half one, it will cause SiC particles pulling out and lead to pits on the surface. Furthermore, if the pulling out SiC particles are pressed into Al matrix by abrasive particle again, it may cause protruding of sic particles. In addition, when the tensile stress is very large, the serious interface debonding will cause the protruding of SiC particles under the Al matrix as well, as shown in **Fig. 8i**.

The phenomenon of Al matrix covering can be seen in **Fig. 8k** and **l**. That is because the extrusion of Al-matrix between the SiC particles produces secondary shear deformation under the action of abrasive particles being very easy to cover the SiC particles in the direction of cutting. From **Fig. 8l**, it can be seen that the phenomenon of Al-matrix covering is especially serious and this is because the high volume fraction of SiC particles make the deformation of Al-matrix be hindered and the excessive shear stress make the phenomenon of Al-matrix tearing be more serious. There are many pits and cracks in the cladding, as shown in **Fig. 8m**, causing the weak bonding strength and making the SiC particles easy to break off. After cleaning the SiCp/Al composites with ultrasonic washer for 10 minutes, most of the surface claddings shown in **Fig. 8n** are cleared, showing the broken particles and cladding fracture surface, as shown in **Fig. 8m** and **l**. Thus, it can be seen that the cladding formed by plastic deformation of Al-matrix in the cutting of SiCp/Al composites process is also an important defects influencing the surface quality.

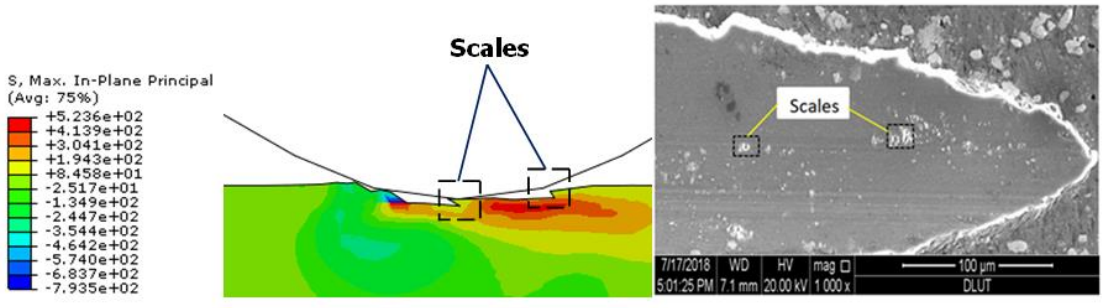

(a) (b)

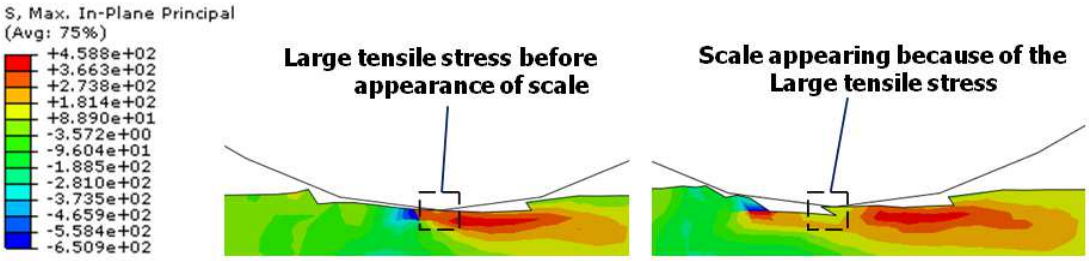
S, Max. In-Plane Principal
(Avg: 75%)
+4.588e+02
+3.663e+02
+2.738e+02
+1.814e+02
+8.890e+01
-3.572e+00
-9.604e+01
-1.885e+02
-2.810e+02
-3.735e+02
-4.659e+02
-5.584e+02
-6.509e+02
Large tensile stress before appearance of scale
Scale appearing because of the Large tensile stress

(c) (d)

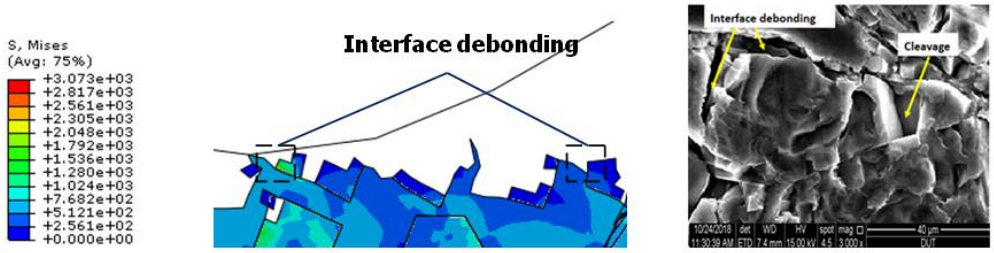
S, Mises
(Avg: 75%)
+3.073e+03
+2.817e+03
+2.561e+03
+2.305e+03
+2.048e+03
+1.792e+03
+1.536e+03
+1.280e+03
+1.024e+03
+7.682e+02
+5.121e+02
+2.561e+02
+0.000e+00
Interface debonding
Interface debonding
Cleavage

(e) (f)

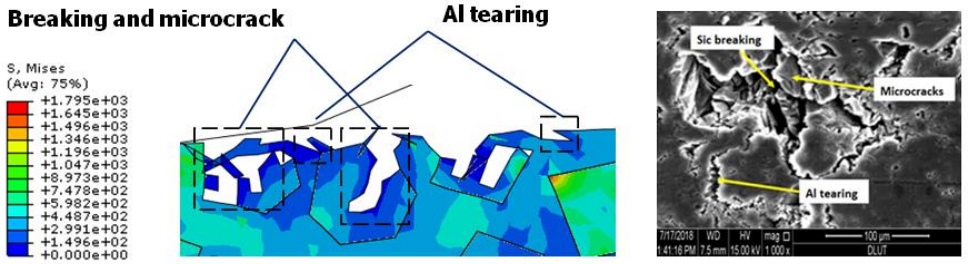
Breaking and microcrack
Al tearing
S, Mises
(Avg: 75%)
+1.795e+03
+1.645e+03
+1.496e+03
+1.346e+03
+1.196e+03
+1.047e+03
+8.973e+02
+7.478e+02
+5.982e+02
+4.487e+02
+2.991e+02
+1.496e+02
+0.000e+00
Sic breaking
Microcracks
Al tearing

(g) (h)

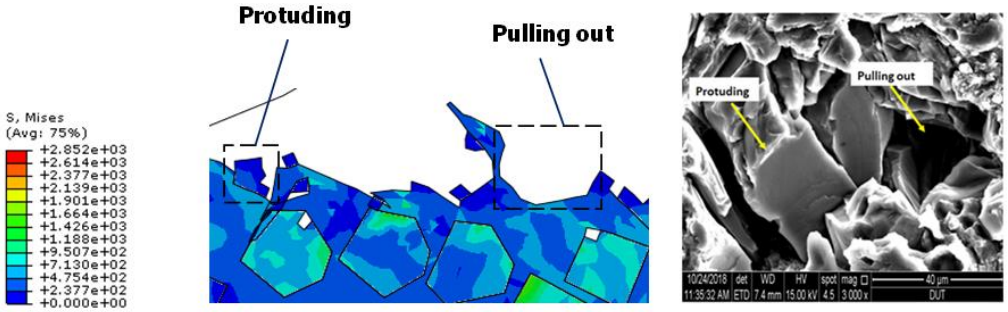
Protuding
Pulling out
S, Mises
(Avg: 75%)
+2.852e+03
+2.614e+03
+2.377e+03
+2.139e+03
+1.901e+03
+1.664e+03
+1.426e+03
+1.188e+03
+9.507e+02
+7.130e+02
+4.754e+02
+2.377e+02
+0.000e+00
Protuding
Pulling out

(i) (j)

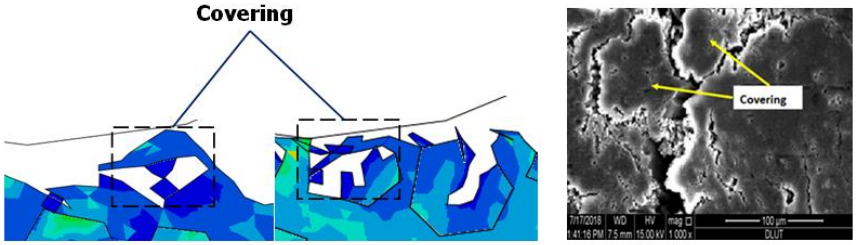
Covering
Covering

(k) (l)

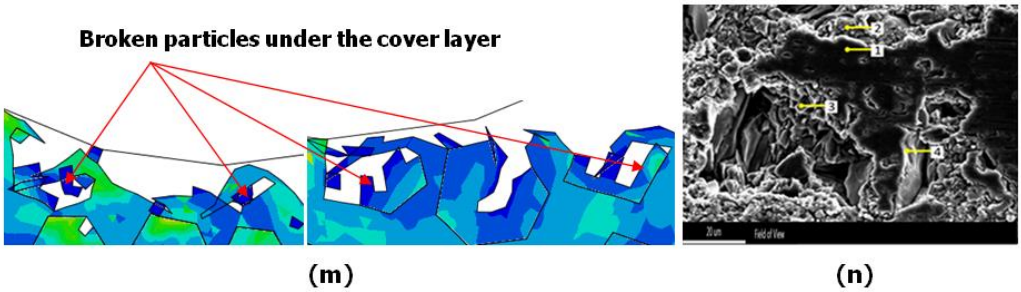

Fig. 8 Removal models of 2A12 Al, silicon carbide and 65% SiCp/Al composites by simulation and experiment: a-d 2A12 Al, e,f silicon carbide, g-n 65% SiCp/Al composites

The different positions tagged in the **Fig. 8n** are analyzed by energy dispersive spectroscopy (EDS) and the major elements are identified, as shown in **Fig. 9**. It can be seen that the main elements of position tagged number 1 is Al. The position tagged number 2 has the highest amount of Al and the next is silicon. The major elements of position tagged number 3 and 4 are silicon. Thus, the energy spectrum analysis results show that bellowing the cladding is broken SiC particles and the cladding consists of Al-matrix and clastic SiC particles within it, verifying the inference of preceding part of the text.

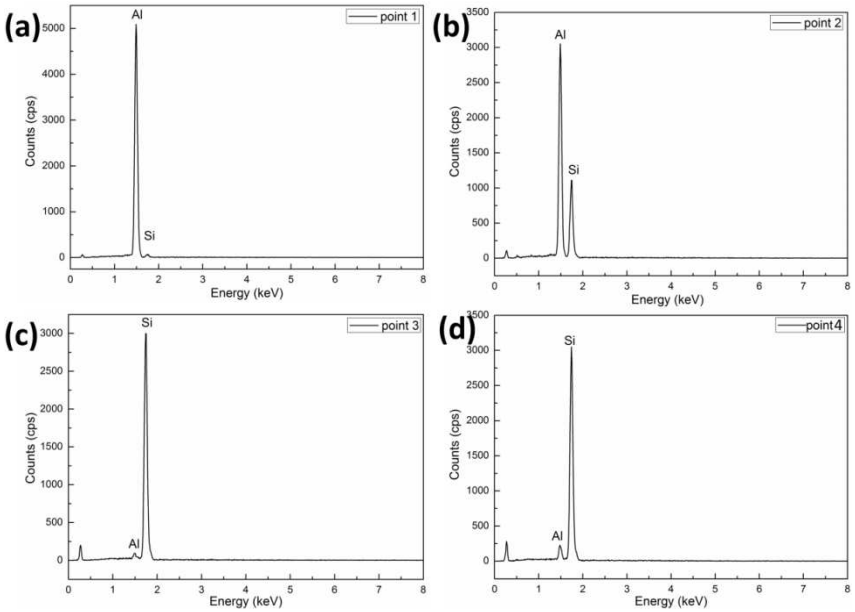

Fig. 9 the result of energy spectrum analysis on cover layer

5 Conclusions

In this paper, the single point cutting simulation and experiments were conducted for high-volume fraction SiCp/Al composites and Al alloy. The surface topography was observed, and the surface formation characteristics of 65% SiCp/Al composites were analyzed. Good agreement was found between the experimental and calculated results. The following conclusions can be drawn:

1) The removal characteristics of SiCp/Al composites are different from the Al alloy materials. In the cutting process of SiCp/Al composites, there are plastic deformation, ploughing and cumulating of Al alloy, and

slippage, detachment and crushing of SiC particles.

2) The high-volume SiC particles increase the brittleness and cause the defects like interfacial debonding, al tearing, protruding, and pulling out, crushing, part crushing, and so on. These defects make the profile fluctuate widely. Thus, it lowers the surface quality and profile dimensional accuracy of SiCp/Al composites.

3) With the cutting depth increases, fluctuations of SiCp/Al profile becoming larger. The range is zero to 8 μm when the cutting depth increased gradually to 20μm.

4) There are thin and discrete layers covered on the machined surface. The layers consist of Al-matrix and clastic SiC particles.

Funding information

This research was supported financially by National Natural Science Foundation of China (NSFC) (Projects no. 51875079, U1908228) and Liaoning province "Xingliao Talents Program" young top talent (Projects no. XLYC1907196).

References:

[1] Rahman MH, Rashed HM(2014) Characterization of Silicon Carbide Reinforced Aluminum Matrix Composites. Procedia Engineering; 90: 103-109

[2] İzciler M, Muratoglu M(2003) Wear behaviour of SiC reinforced 2124 Al alloy composite in RWAT system. J Mater Process Tech; 132(1–3): 67-72

[3] Lou HS, Qu SG, Li XQ, Wang B, Kuang TR(2016) Glass coating on SiCp /Al composite mirror for ultra-smooth surface. Int J Adv Manuf Tech; 88(5-8): 1745-1753

[4] Kevorkijan VM(1999) Aluminum composites for automotive applications: a global perspective. Jom-Us 51(11):54–58

[5] Lee HS, Jeon KY, Kim HY, Hong SH(2000) Fabrication process and thermal properties of SiCp/Al metal matrix composites for electronic packaging applications. J MATER SCI 35(24):6231–6236

[6] Cui Y, Wang LF, Ren JY(2008) Multi-functional SiC/Al composites for aerospace applications. CHINESE J AERONAUT 21(6):578–584

[7] Zhang H(2013) Experimental Investigation on Ultrasonic Vibration-Assisted Turning of SiCp/Al Composites. MATER MANUF PROCESS 28(9): 999-1002

[8] Ahamed AR, Asokan P, Aravindan S, Prakash, MK(2010) Drilling of hybrid Al-5%SiCp-5%B4Cp metal matrix composites. INT J ADV MANUF TECH 49(9-12): 871-877

[9] Kadivar MA, Akbari J, Yousefi R, Rahi, A,Nick, MG(2014) Investigating the effects of vibration method on ultrasonic-assisted drilling of Al/SiCp metal matrix composites. ROBOT CIM-INT MANUF 30(3): 344-350

[10] Zhou L, Huang S, Xu L, Bai D, Zhao P(2013) Drilling characteristics of SiCp/Al composites with electroplated diamond drills. INT J ADV MANUF TECH 69(5-8): 1165-1173

[11] Xiong Y, Wang W, Jiang R, Lin K , Song G(2016) Surface integrity of milling in-situ TiB2 particle reinforced Al matrix composites. INT J REFRACT MET H 54: 407-416

[12] Wang YF, Liao WH,Y ang K, Teng XY, Chen WQ(2019) Simulation and experimental investigation on the cutting mechanism and surface generation in machining SiCp /Al MMCs. INT J ADV MANUF TECH 100(5–8),1393–1404

[13] Liu J, Cheng K, Ding H, Chen S, Zhao L(2016) An Investigation of Surface Defect Formation in Micro Milling the 45% SiCp/Al Composite. Procedia Cirp 45: 211-214

[14] Wu Q, Xu W, Zhang L(2018) A micromechanics analysis of the material removal mechanisms in the cutting of ceramic particle reinforced metal matrix composites. MACH SCI TECHNOL 22(4): 638-651

[15] Xiang DH, Shi ZL, Feng HR, Wu BF, Zhang ZM, Chen YB, Niu XX, Zhao B(2019) Finite

element analysis of ultrasonic assisted milling of SiCp/Al composites. INT J ADV MANUF TECH 105(7–8):3477–3488

[16] Wang YF, Liao WH, Yang K, Chen WQ, Liu TT(2019) Investigation on cutting mechanism of SiCp/Al composites in precision turning. INT J ADV MANUF TECH 100(1-4):963-972

[17] Yan C, Zhang L(1994) Single-point scratching of 6061 Al alloy reinforced by different ceramic particles[J]. Applied Composite Materials 1(6): 431-447

[18] Feng PF, L GQ, Zhang JF(2014) Ultrasonic vibration-assisted scratch characteristics of silicon carbide-reinforced aluminum matrix composites[J]. Ceramics International 40(7): 10817-10823

[19] Zha HT, Feng PF, Zhang JF(2018) Material removal mechanism in rotary ultrasonic machining of high-volume fraction SiCp/Al composites[J]. International Journal of Advanced Manufacturing Technology 97(5-8): 2099-2109

[20] Shan HL, Guo RX, Xia HT(2009) Numerical simulation of random distribution model of particle reinforced composites [J] Science and Technology and Engineering 9(10) 2724-2727.

[21] Zhu Y, Kishawy HA(2005) Influence of alumina particles on the mechanics of machining metal matrix composites, Int. J. Mach. Tools Manuf. 45 389–398.

[22] Pramanik A, Zhang LC, Arsecularatne JA(2007) An FEM investigation into the behavior of metal matrix composites: Tool–particle interaction during orthogonal cutting. INT J MACH TOOL MANU 47(10): 1497-1506

[23] Dandekar CR, Shin YC(2009) Multi-step 3-D finite element modeling of subsurface damage in machining particulate reinforced metal matrix composites. COMPOS PART A-APPL S 40(8): 1231-1239

[24] Fathipour M, Zoghipour P, Tarighi J, Yousefi R(2012) Investigation of reinforced sic particles percentage on machining force of metal matrix composite.Mod Appl Sci 6(8): p9

[25] Fathipour M, Hamedi M, Yousefi R(2013) Numerical and experimental analysis of machining of Al (20 vol% SiC) composite by the use of ABAQUS software. MATERIALWISS WERKS 44(1): 14-20

[26] Li(2006) Experimental study on the constitutive relationship of 2A12 aluminum alloy. Harbin Institute of Technology

[27] Zhou L, Huang ST, Wang D, Yu XL(2011) Finite element and experimental studies of the cutting process of Si Cp/Al composites with PCD tools. INT J ADV MANUF TECH 52(5-8): 619-626

[28] Zhang W, Wei G, Xiao XK(2013) Constitutive relation and failure model of 2A12 aluminum alloy. Acta Armamentarii 34(3):276-282

[29] Liu J, Bai YL, Xu CY(2014) Evaluation of ductile fracture models in finite element simulation of metal cutting processes. J MANUF SCI E-T ASME 136(1): 011010

[30] Zhou L, Cui C, Zhang PF, Ma ZY(2016) Finite element and experimental analysis of machinability during machining of high-volume fraction SiCp/Al composites. INT J ADV MANUF TECH 91(5-8):1935-1944

[31] Hibbitt, Karlsson, Sorensen(2001) ABAQUS/Explicit: User's Manual, Hibbitt, Karlsson and Sorensen Incorporated

[32] Hibbitt, Karlsson, Sorensen(2006) Abaqus/Explicit Theory and User Manuals. Version 6.6.1.

[33] Kan Y, Liu ZG, Zhang SH,Zhang LW, Cheng M, Song HW(2014) Microstructure-Based Numerical Simulation of the Tensile Behavior of SiC/Al Composites. J MATER ENG PERFORM 23(3):1069-1076

[34] Zhou L, Wang Y, Ma ZY, Yu XL(2014) Finite element and experimental studies of the formation mechanism of edge defects during machining of Si Cp/Al composites. INT J MACH TOOL MANU 84: 9-16

Figures

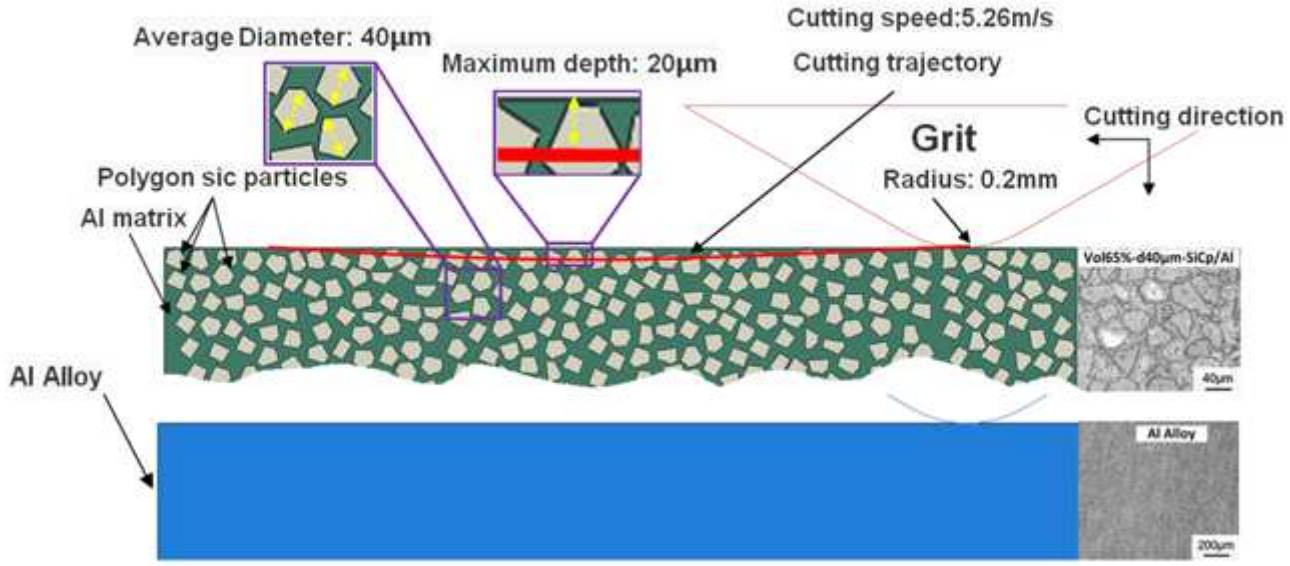

Figure 1

Finite element model of single point cutting of 65% SiCp/Al composites and 2A12 aluminum alloy

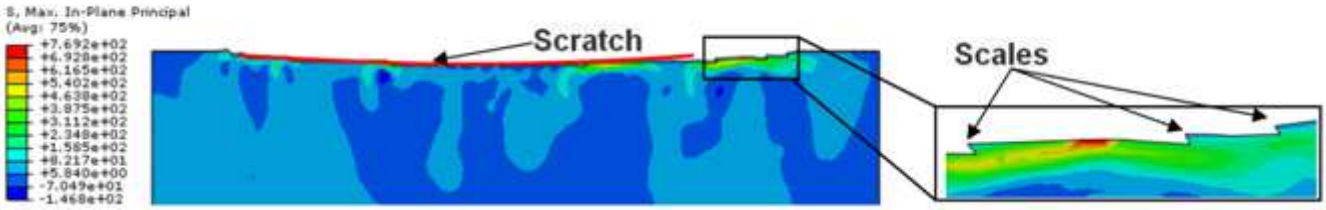

Figure 2

Removal models of 2A12 aluminum alloy materials

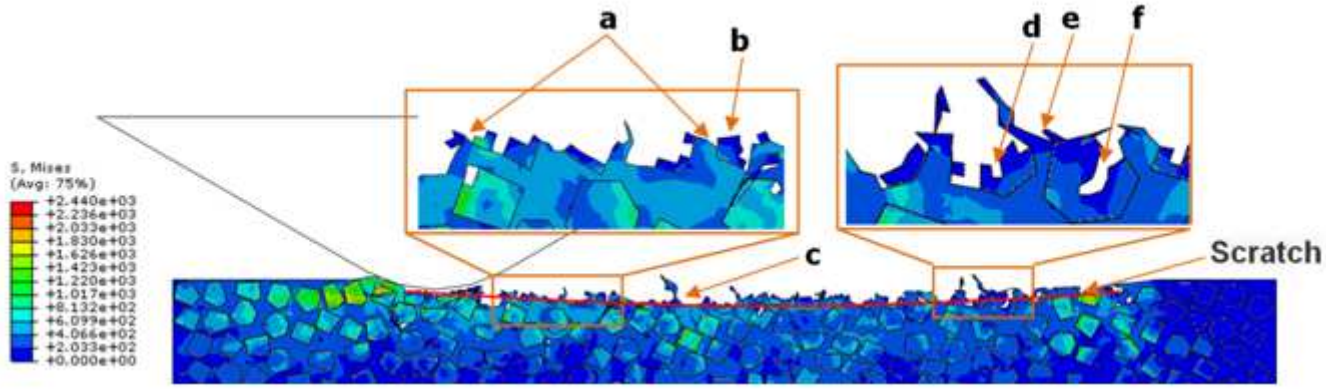

Figure 3

Removal models of 65% SiCp/Al composites

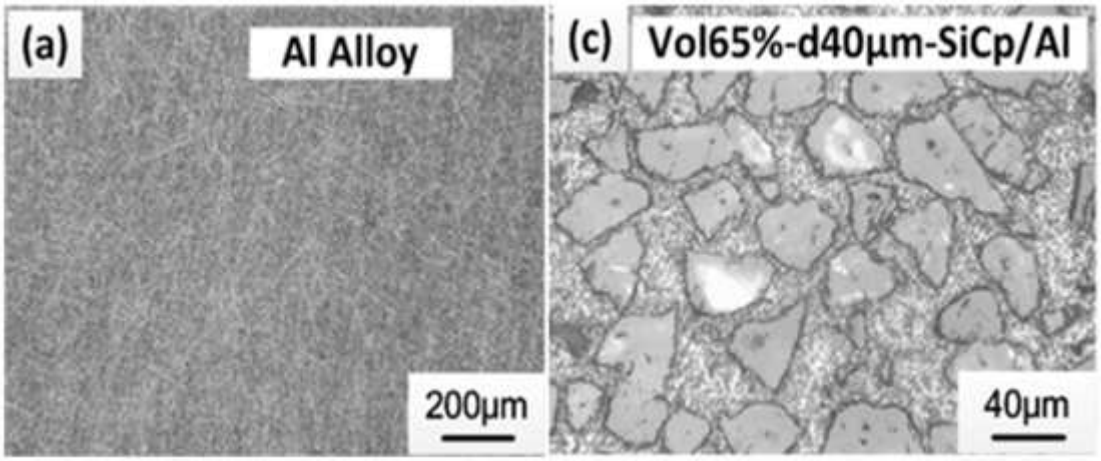

Figure 4

Surface topography of test pieces after pretreatment

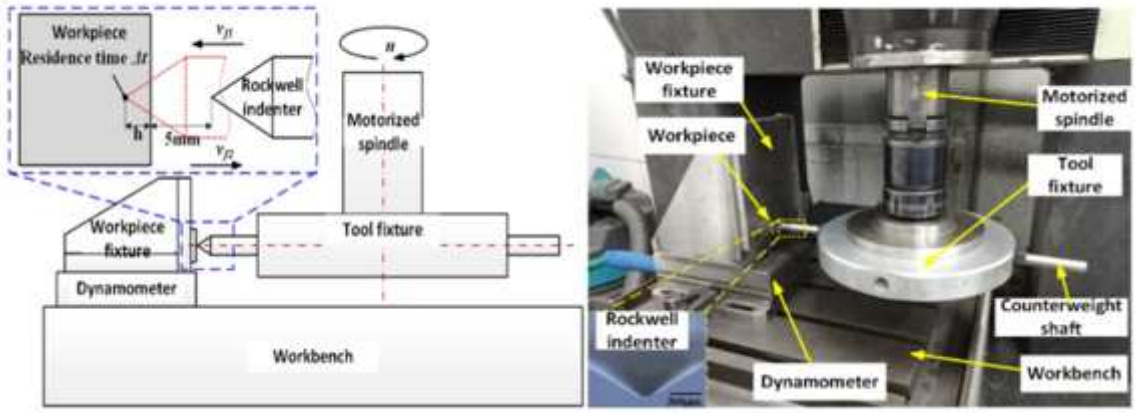

Figure 5

The method of dicing test and testing apparatus

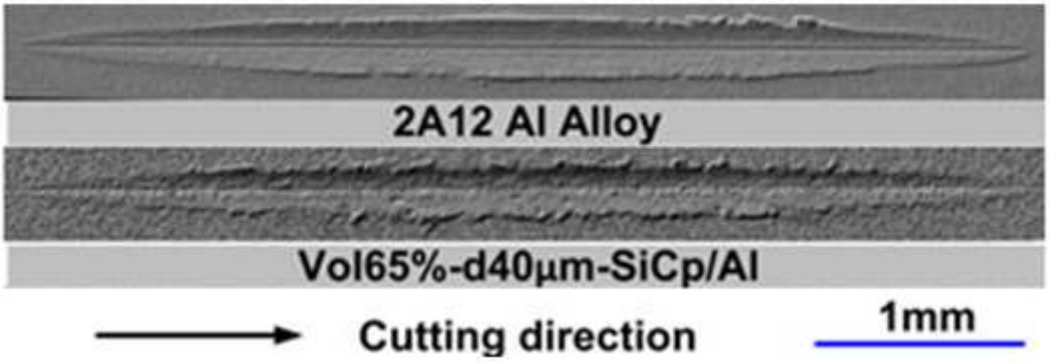

Figure 6

The overall appearance of three materials after dicing

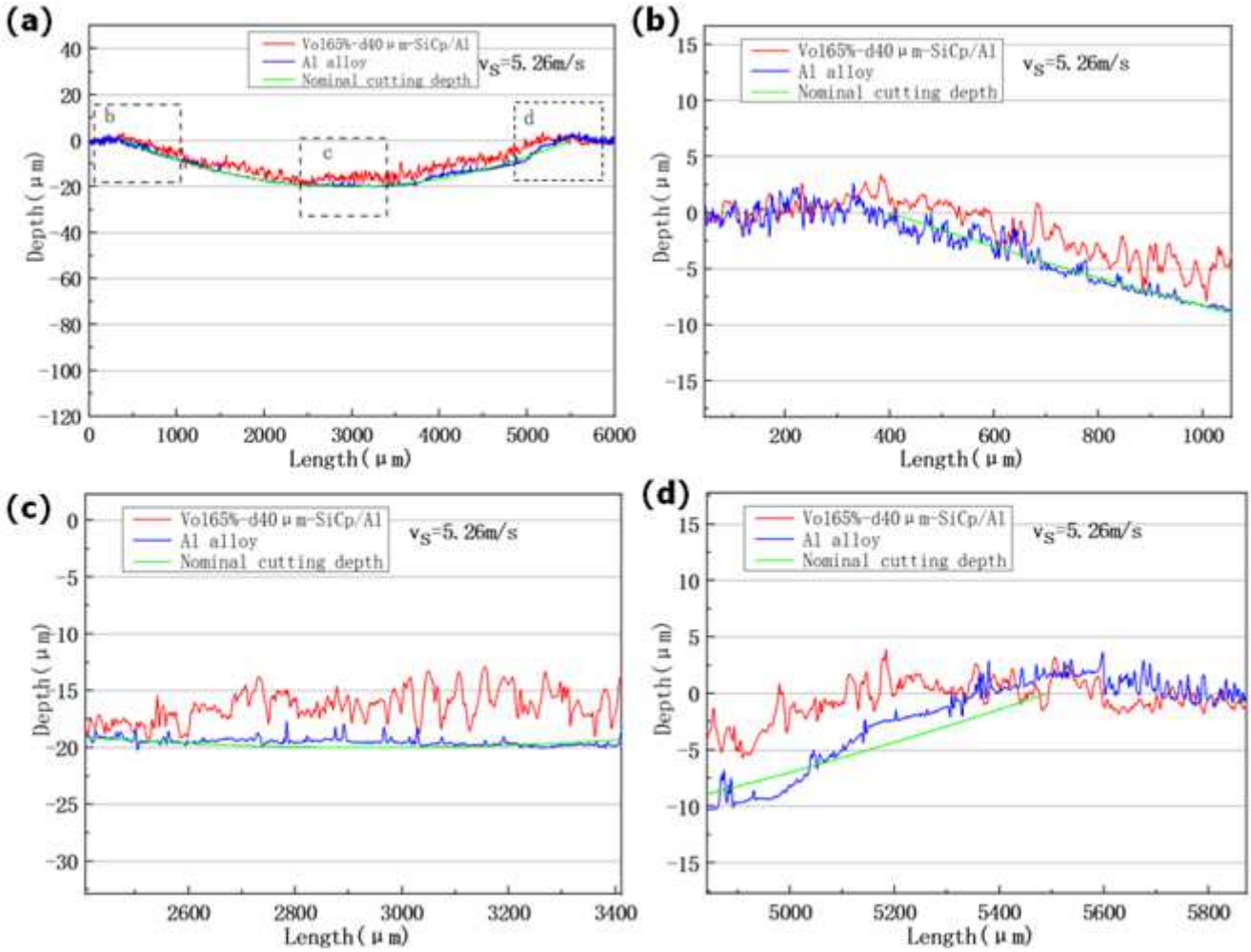

Figure 7

The scratch profile dimensions of three materials after dicing

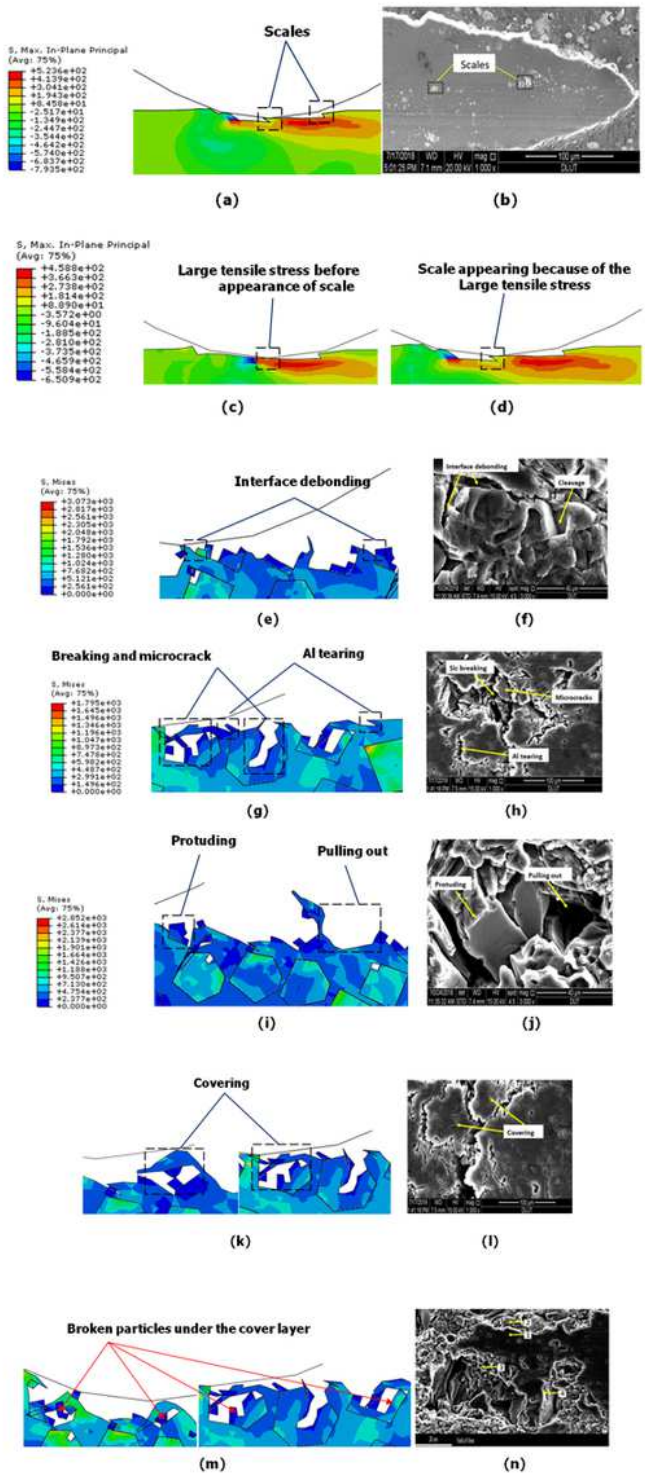

Figure 8

Removal models of 2A12 Al, silicon carbide and 65% SiCp/Al composites by simulation and experiment: a-d 2A12 Al, e,f silicon carbide, g-n 65% SiCp/Al composites

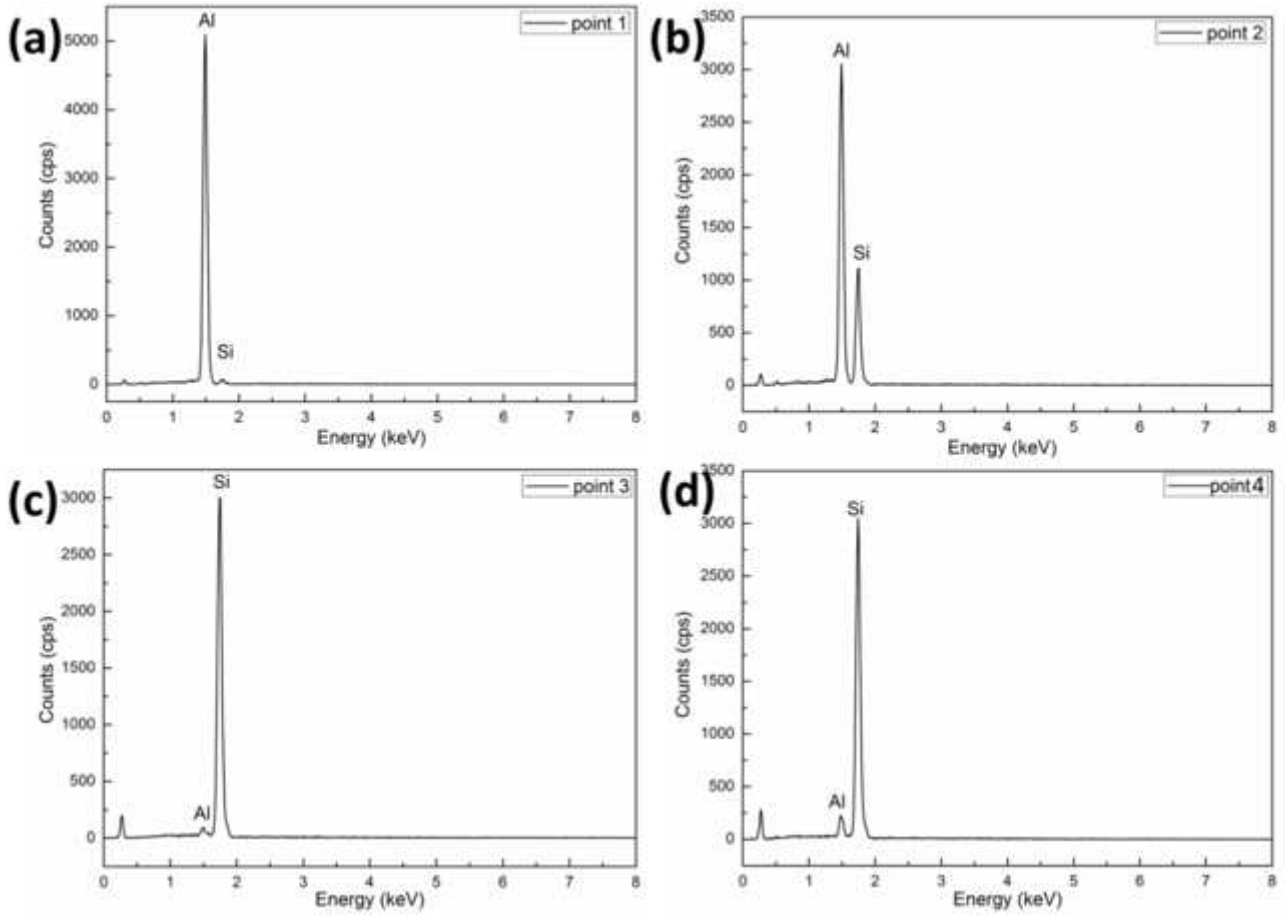

Figure 9

the result of energy spectrum analysis on cover layer